Organic Electronics 81 (2020) 105675

Contents lists available at ScienceDirect

Organic Electronics

journal homepage: http://www.elsevier.com/locate/orgel

Modification of interface between PEDOT:PSS and perovskite film inserting an ultrathin LiF layer for enhancing efficiency of perovskite light-emitting diodes

Zongtao Li [a,b], Kai Cao [a], Jiasheng Li [a,b,*], Xuewei Du [a], Yong Tang [a], Binhai Yu [a]

[a] Engineering Research Center of Green Manufacturing for Energy-Saving and New-Energy Technology, South China University of Technology, Guangdong, 510640, China

[b] Foshan Nationstar Optoelectronics Company Ltd., Foshan, 528000, China

ARTICLE INFO

Keywords:
Perovskite
Light-emitting diodes
PEDOT:PSS
Interface modification

ABSTRACT

PEDOT:PSS has been widely used in perovskite light-emitting diodes (PeLEDs) due to its high hole current conductivity and work function. However, the unbalanced charge injection and severe exciton quenching in PEDOT:PSS restrict the EL performance of PeLEDs. In this work, a facile interface modification method is introduced in which an ultrathin LiF layer is inserted at the interface between PEDOT:PSS and $MAPBBr_3$ perovskite film. Our results indicate that the inserted ultrathin LiF layer contributes to an efficient interface passivation effect between the PEDOT:PSS layer and the perovskite film, which significantly suppresses both the exciton quenching by the conductive PEDOT chains and the perovskite film defect density at the interface. Moreover, balanced charge injection is realized by adjusting the thickness of the LiF layer, which also serves as an electron blocking layer, in order to preferentially hinder electron current over hole current. Consequently, the optimal PeLED with a 2 nm LiF layer exhibits a significantly decreased turn-on voltage of 2.8 V compared to 4.9 V of the pristine device without a LiF layer, combined with an over 100-fold enhancement in the maximum luminance (10415 cd/m^2), current efficiency (12.1 cd/A), and external quantum efficiency (3.5%).

1. Introduction

Perovskites have been used prominently in light-emitting diodes (LEDs) [1–3], solar cells [4–6], and photodetectors [7–9] due to their excellent photoelectrical and solution processability properties. The external quantum efficiency (EQE) of perovskite LEDs (PeLEDs) has increased from 0.1% in the first device [1] to a high EQE of over 20% [10–14] in recent years. This increase is mainly due to improved photon management [10–12,15] and defect passivation in perovskite crystals [13,14,16,17] by using additives such as TPBi, BCP, BTBABr, and others. Generally, non-radiative recombination is induced by defects occuring at the boundaries of the perovskite crystals and the interface between the perovskite emitting layer (EML) and the carrier transport layer (CTL) [18–21].

PEDOT:PSS is one of the most promising HTL materials for PeLEDs due to its excellent hole transport ability, high transmittance and flexibility, and relatively high work function [22,23]. However, there are still some shortcomings that limit the efficiency of PeLEDs using PEDOT:PSS as the HTL. Firstly, the direct contact between highly conductive PEDOT chains and the perovskite film leads to severe exciton quenching [24,25]. Secondly, the energy barrier between the work function of PEDOT:PSS (~5.0 eV) and the highest occupied molecular orbital (HOMO) of perovskite (~5.7 eV) is so large that the injection of hole current into the perovskite layer is heavily suppressed [26,27]. Thirdly, the polycrystalline perovskite films that are spin-coated on the surface of conventional PEDOT:PSS usually have poor morphology, which may lead to huge leakage current and degraded device performance [28,29]. Therefore, the surface defects and morphology of PEDOT:PSS should be improved.

One efficient method to solve the above issues is the additive engineering of PEDOT:PSS. Cho et al. [2] modified the self-organized conductive polymer by adding tetrafluoroethylene-perfluoro-3,6-dioxa-4-methyl-7-octene-sulfonic acid copolymer (PFI) into PEDOT:PSS solution to increase the work function (WF), and successfully

* Corresponding author. Engineering Research Center of Green Manufacturing for Energy-Saving and New-Energy Technology, South China University of Technology, Guangdong, 510640, China.
E-mail address: mejiashengli@mail.scut.edu.cn (J. Li).

https://doi.org/10.1016/j.orgel.2020.105675
Received 11 November 2019; Received in revised form 14 January 2020; Accepted 15 January 2020

fabricated the first high-efficiency PeLED with 8.53% EQE. However, the conductivity of PEDOT:PSS decreased with increasing incorporation of PFI, limiting the further improvement of device performance. Other additives such as Au-nanoparticles [24], Nafion [30] and SDBS [31] were used to increase the conductivity of PEDOT:PSS. However, the large energy offset remains unchanged, which is detrimental to effective charge injection. To achieve the synergistical improvement of both WF and conductivity of PEDOT:PSS, Lee et al. [32] added both MABr and PFI into the solution and successfully decoupled the WF and conductivity. With this strategy, the PeLED with high current efficiency of 52.86% was fabricated. However, the increased category of additives inevitably increases the complexity of the PEDOT:PSS solution, which imposes limitations on the fabrication process. Another effective method to modify the PEDOT:PSS is to insert a buffer layer such as TFB [33], Di-NPB [34], PTAA [35] and PVK [36] between the PEDOT:PSS and the perovskite film. These interlayer buffers can efficiently reduce the energy barrier between the PEDOT:PSS and the perovskite layer because of their deeper HOMO compared to PEDOT:PSS, and achieve balanced current injection and transport due to the lowered hole injection barrier. However, most of these organic polymers have low resistance to strong nonpolar solvents. This places restrictions in the fabrication process of the perovskite films, for example by precluding the use of the anti-solvent method.

In this work, a facile interface engineering method is adapted by inserting an ultrathin LiF layer (high resistance of solvents) between PEDOT:PSS and the archetype 3D perovskite film of methylammonium lead tribromide (MAPbBr3). The influence of the LiF layer on the PEDOT:PSS and perovskite film morphology, as well as the photoluminance (PL) of the perovskite film are studied by adjusting the thickness of the LiF layer. The electroluminescence (EL), including the hole/electron defects and the injection balance, of PeLEDs employing LiF layers of different thicknesses are then measured. The optimal device with 2 nm LiF layer exhibits an over 100-fold enhancement in the maximum luminance (10415 cd/m^2), current efficiency (CE) (12.1 cd/A) and external quantum efficiency (EQE) (3.5%), as well as a lower open voltage of 2.8 V compared to the 4.9 V of the reference device.

2. Experiment section

2.1. Materials

PEDOT:PSS Celvios P Al 4083 (4083) was purchased from Heraeus Electronic Materials Division. Methylammonium bromide (MABr, >99.99%), lead bromide ($PbBr_2$, >99.99%) and TPBi (>99%) were purchased from Xi'an Polymer Light Technology Corp. DMF, DMSO and chlorobenzene (HPLC, >99.9%) were purchased from Aladdin. All chemicals were used as received without further purification.

2.2. PeLED fabrication

Patterned ITO substrates were cleaned using toluene, isopropanol and ethanol in a sonic bath successively, followed by drying in a vacuum oven. Prior to device fabrication, the substrates were treated by argon plasma for 30 s. PEDOT:PSS was spin-coated on the ITO substrates at 4000 rpm, followed by baking at 120 °C for 15 min under ambient conditions. The substrates were then transferred into a vacuum chamber inside an Ar-filled glovebox (H_2O and $O_2 \leq 0.1$ ppm), followed by thermal evaporation of LiF (1 nm–4 nm) at an evaporation rate of 0.1 Å/s. The perovskite precursor solution (20 wt%) was prepared by dissolving MABr and $PbBr_2$ at the molar ratio of 1.1:1 in DMF/DMSO mixed solution (V_{DMF}: V_{DMSO} = 7:3). To form the perovskite layer, 75 μL precursor solution was spin-coated on ITO/PEDOT:PSS/LiF substrates at a speed of 3000 rpm for 60 s. After 15 s of spin-coating, 50 μL chlorobenzene was quickly dropped onto the center of the substrates, followed by baking at 60 °C for 10 min. TPBi (60 nm), LiF (1.5 nm) and Al (100 nm) were then successively evaporated on top of the perovskite film under high vacuum of 4×10^{-5} Pa with evaporation rates of 1 Å/s, 0.1 Å/s and 3 Å/s, respectively.

2.3. Characterization

The film thichnesses were measured using an SQC-310C thin film deposition system (Inficon). The AFM images of PEDOT:PSS/LiF layers were obtained using a Bruker edge atomic force microscope. The contact angle of PEDOT:PSS/LiF layers were measured using Dataphysics OCA. The transmittance spectra were recorded using a UV–vis spectrometer (Shimadzu) in the wavelength range from 300 nm to 800 nm at 1 nm intervals. The SEM images of perovskite films were obtained using a field-emission SEM (Zeiss, Merlin). The XRD patterns of perovskite films were measured by a X-ray diffractometer (D8 Advance, Bruker). The PL spectra of the perovskite films were recorded using a fluorescence spectrophotometer (RF-6000, Shimadzu) using a Xe lamp as the excitation source. The time-resolved fluorescence spectra were recorded on a steady-state fluorescence spectrometer (FLS1000, Edinburgh). The impedance measurements were conducted using a DH7000 electrochemical workstation. The current density (J)-bias (V)- luminance (L) measurements were performed using a Keithley 2450 source meter and a Konica Minolta Chroma Meter CS-200. The EL spectra were recorded by a PhotoResearch PR-705 photometer. The EQE was calculated from the luminance, current density and EL spectra data assuming a Lambertian distribution.

3. Results and discussion

The morphology of PEDOT:PSS films with different thicknesses of LiF was observed by AFM as shown in Fig. 1(a–e). The relationship between the RMS roughness of PEDOT:PSS and the thickness of LiF is plotted in Fig. 1(f). Compared to the pristine film, the 1 nm thick LiF layer on the surface of PEDOT:PSS effectively decreases the surface RMS roughness from 2.48 nm to 1.29 nm, thereby improving the electrical contact between PEDOT:PSS and the perovskite layer. As we know, PEDOT:PSS film comprises of conductive PEDOT chains in the bulk and insulated PSS chains at the surface. The direct contact of the PEDOT chains and perovskite film leads to exciton dissociation and nonradiative recombination. Li and coworkers [3] demonstrated that PEDOT:PSS film is rough and the perovskite crystals can fill into the voids at the surface of PEDOT:PSS. We postulate that the higher RMS roughness of the pristine film reflects the uneven distribution of the PSS chains, and the evaporation of 1 nm thick LiF can effectively fill the PEDOT:PSS voids on the film surface. As a result, applying a thin LiF layer at the surface of PEDOT:PSS not only improves the surface morphology but also prevents the direct contact of the conductive PEDOT chains and perovskite film. The surface roughness of the PEDOT:PSS/LiF film increases gradually with further increase of the LiF thickness. The surface roughness of PEDOT:PSS with 2 nm, 3 nm and 4 nm thick LiF is 1.58 nm, 2.25 nm and 2.26 nm respectively. The increase in surface roughness is due to the random directional distribution of the evaporated LiF.

The top view SEM images of perovskite films prepared on ITO/PEDOT:PSS substrates with different thicknesses of the LiF layers are shown in Fig. 1(a'-e'). All perovskite films were prepared by adopting the anti-solvent method with chlorobenzene as the nonpolar solvent. As shown in Fig. 1(a'), perovskite film prepared on ITO/PEDOT:PSS substrate exhibits a poor morphology with voids and pinholes. However, these pinholes are absent for the perovskite films prepared on ITO/PEDOT:PSS/LiF substrates with LiF layers, while the grains become large and amorphous. The density and uniformity of the perovskite films increase with the LiF thickness. This is beneficial for the suppression of leakage current. XRD results are presented to demonstrate the improvement of the perovskite film quality (Fig. S1). $CH_3NH_3PbBr_3$ films prepared on ITO/PEDOT:PSS substrates without and with LiF layers exhibit the same diffraction peak positions at 15.04°, 30.24° and 45.97°, which can be assigned to the (100), (200) and (300) planes of the

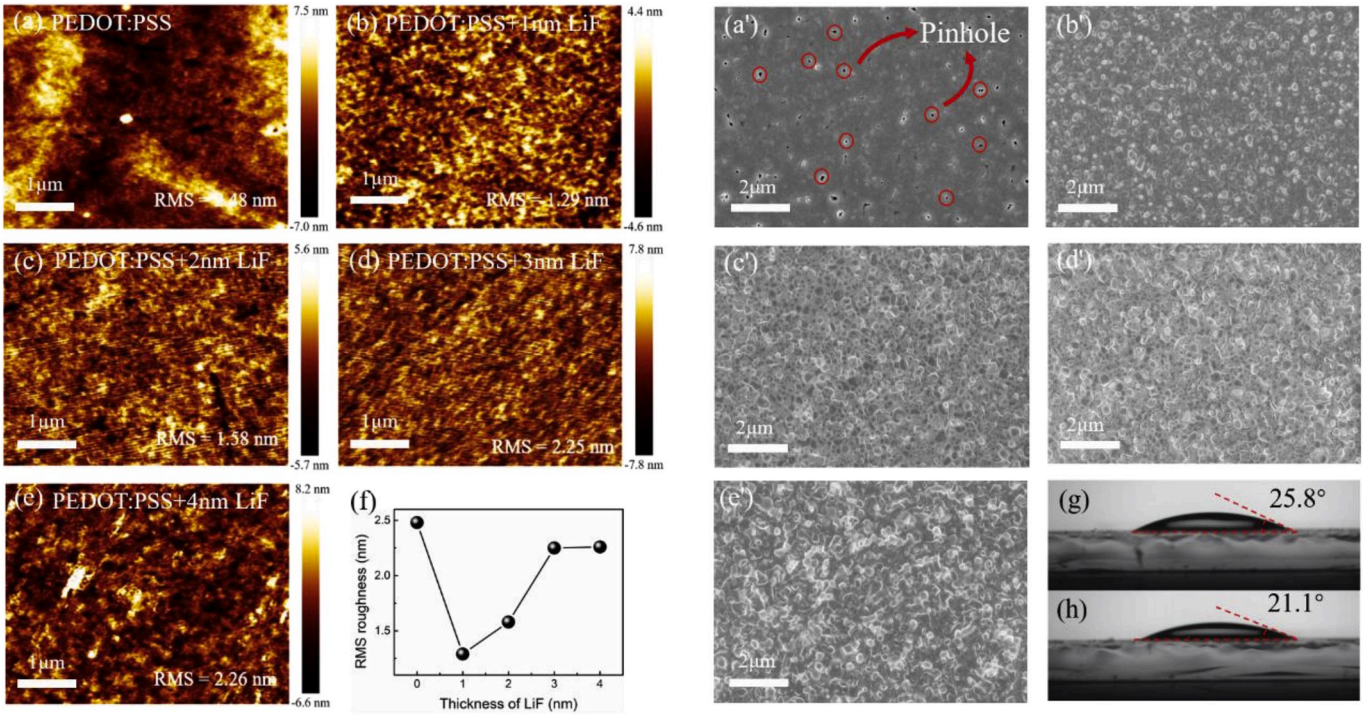

Fig. 1. (a-e) Atomic force microscope (AFM) images of ITO/PEDOT:PSS/LiF films with LiF thicknesses from 0 to 4 nm, respectively. (a'-e') Top view scanning electron microscope (SEM) images of perovskite films on ITO/PEDOT:PSS/LiF (0–4 nm) with LiF thicknesses from 0 to 4 nm, respectively. (f) The surface RMS roughness of ITO/PEDOT:PSS/LiF films verses LiF layer thickness. (g-h) The contact angles of mixed DMF/DMSO solution on (g) ITO/PEDOT:PSS substrate and (h) ITO/PEDOT:PSS/2 nm LiF substrate.

cubic MAPbBr3 phase, respectively. However, the intensities of these peaks increase significantly for substrates modified by LiF layers, demonstrating that the LiF layers have enhanced the crystallinity of the perovskite films. The wettability of ITO/PEDOT:PSS substrates without and with LiF layers were also investigated as shown in Fig. 1(g) and Fig. 1(h), respectively. The contact angle of mixed DMF/DMSO solution on the ITO/PEDOT:PSS substrate is 25.8°, and decreases to 21.1° on the substrate modified by the LiF layer. The decreased contact angle indicates the improved wetting property of PEDOT:PSS modified by the LiF layer. This improved wetting property is beneficial for the deposition

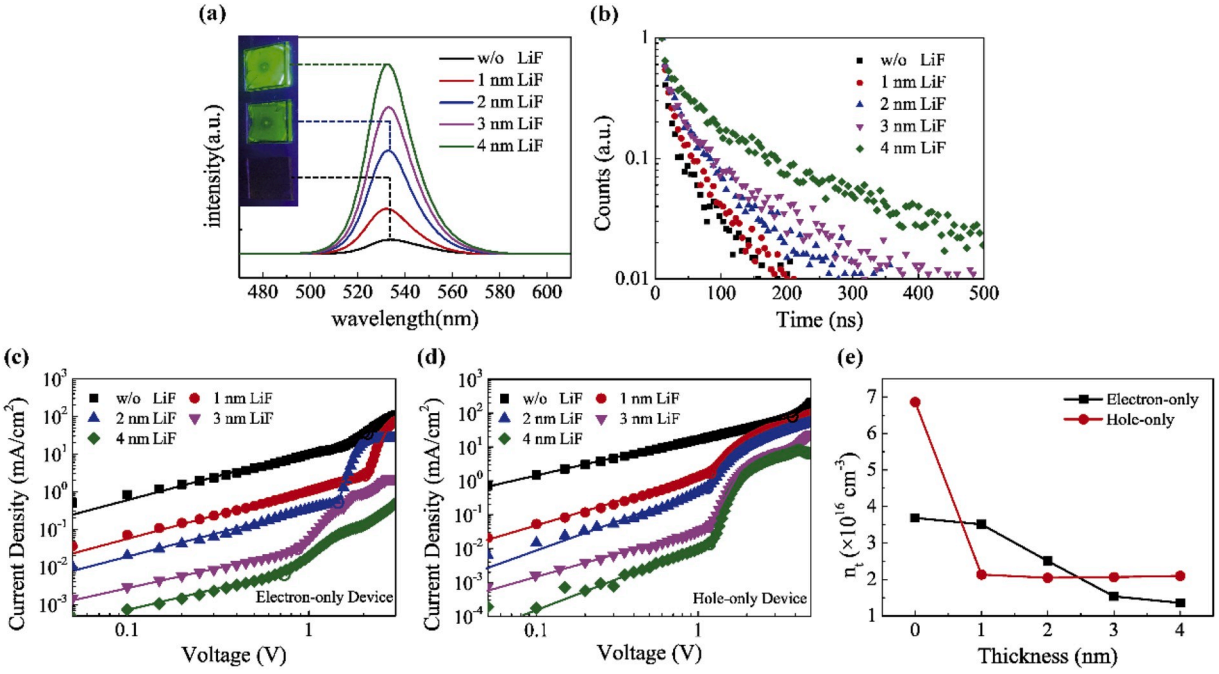

Fig. 2. Normalized steady-state (a) and time-resolved (b) PL spectra of perovskite film deposited on ITO/PEDOT:PSS/LiF substrates with different LiF thicknesses. Dark current-voltage curves from (c) electron-only and (d) hole-only devices with LiF thicknesses varied from 0 nm to 4 nm. (e)The electron and hole trap states of perovskite film calculated from the dark J-V curves versus the LiF thickness.

of perovskite films from mixed DMF/DMSO solution and improves the film morphology. However, the grain sizes of the perovskite film become larger and more unevenly distributed when the LiF thickness is further increased to 4 nm, which leads to an increased surface roughness. Therefore, an optimal LiF thickness on PEDOT:PSS can improve the morphology of the perovskite film. In addition, it is important to note that the LiF ultrathin film is nearly intact after spin coating the perovskite precursor solution. As shown in Fig. S2, the transmittance spectra of the glass/LiF substrate before and after washing by DMF/DMSO mixed solution and chlorobenzene overlap, indicating that the LiF only exists at the interface between the PEDOT:PSS and the perovskite film.

The influence of the LiF modified layer on the optical characteristics of the perovskite film is investigated. The PL spectra of perovskite films deposited on ITO/PEDOT:PSS substrates with different LiF thicknesses are given in Fig. 2(a). Perovskite films deposited on ITO/PEDOT:PSS/LiF substrates have the same PL peaks at 534 nm regardless of the LiF thickness, indicating that the LiF modified layer has negligible effect on the crystal phase. However, the PL intensity is successively enhanced with increasing LiF thickness, demonstrating that the LiF layer contributes to an interface passivation effect. The results of the steady-state and time-resolved PL measurements carried out at an excitation wavelength of 365 nm to investigate the interface passivation effect are shown in Fig. 2(b). The PL decay spectra can be well-fitted to the following equation:

$$A = f_1 e^{-t_1/\tau_1} + f_2 e^{-t_2/\tau_2}, \quad (1)$$

where A is the normalized PL intensity, and the fast PL lifetime τ_1 and the slow PL lifetime τ_2 represent the time constants of nonradiative and radiative decay processes, respectively. f_1 and f_2 are the corresponding refraction of these two decay processes. The average PL lifetime can be calculated according to the following equation:

$$\tau_{avg} = f_1\tau_1 + f_2\tau_2, \quad (2)$$

The fitted results of all the samples are shown in Table 1. The perovskite film deposited on ITO/PEDOT:PSS substrate shows the lowest τ_{avg} of 12.75 ns, indicating a trap-mediated recombination process. As the thickness of LiF increases from 1 nm to 4 nm, τ_{avg} increases to 17.46 ns, 25.64 ns, 28.54 ns and 59.08 ns, respectively. The excitons formed in the perovskite film can be easily dissociated by the conductive PEDOT chains. The ultrathin LiF layer evaporated on the surface of PEDOT:PSS prevents direct contact between the PEDOT chains and the perovskite film, suppressing the exciton transfer at the PEDOT:PSS/perovskite interface. As the LiF thickness increases, exciton dissociation is suppressed owing to the increased insulator property of the LiF film. Therefore, the enhanced PL intensity and increased PL lifetime suggest that exciton quenching induced by the PEDOT:PSS layer is successfully alleviated by the LiF modified layer.

To illustrate the interface passivation effect of the LiF modified layers on perovskite films, the dark current of electron-only devices (ITO/ZnO/LiF/perovskite/TPBi/LiF/Al) and hole-only devices (ITO/PEDOT/LiF/perovskite/Ag) with different thicknesses of LiF modified layers are given in Fig. 2(c) and (d), respectively. The J-V curve can be divided into two regions: the linear region at low voltage is regarded as the ohmic contact region, while the region that the J-V curve increases significantly is regarded as the trap-filling region. For each J-V curve in Fig. 2(c) and (d), the two kinds of fitting lines represent the theoretical J-V curves of the ohmic contact region and trap-filling region, respectively. Accordingly, the trapping-filling limited voltages (V_{TFL}), defined as the voltages at the intersections of these two kinds of fitting lines, are obtained from the linearly fitted J-V curves to calculate the trap density. The trap density can be calculated according to the following equation:

$$n_t = \frac{2V_{TFL}\varepsilon\varepsilon_0}{eL^2}, \quad (3)$$

where ε is the relative dielectric constant of MAPbBr3 (25.5 [37]), ε_0 is the vacuum permittivity (8.854×10^{-12} F m^{-1}), e is the elementary charge (1.6×10^{-19} Coulombs) and L is the perovskite layer thickness (~400 nm from Fig. 1(f)). The V_{TFL} of electron-only and hole-only devices modified with different thicknesses of LiF layers were obtained and shown in Fig. 2(e). Without the LiF modified layer, the trap density of the electron-only device is 3.69×10^{16} cm^{-3}, suggesting a large number of defect states in the perovskite film. As the LiF thickness increases, the trap density of electron-only devices reduces gradually from 3.51×10^{16} cm^{-3} for the device with 1 nm LiF layer to 1.35×10^{16} cm^{-3} for the device with 4 nm LiF layer. Similarly, the hole trap density decreases sharply from 6.86×10^{16} cm^{-3} to 2.13×10^{16} cm^{-3} with only 1 nm LiF layer and remains nearly constant when the LiF thickness is further increased. As V_{TFL} corresponds to the ionic and electronic transportation, the reduction of both electron and hole trap densities demonstrates the passivation effect of the LiF modified layer. Since the LiF layer has strong resistance to wetting by the DMF/DMSO mixed solution and chlorobenzene as shown in Fig. S2, the passivation effect occurs mainly for the ionic defects at the interface between the perovskite film and PEDOT:PSS.

To analyze the effect of the LiF modified layer on the electroluminescence (EL) performance, PeLEDs with the conventional structure of ITO/PEDOT/LiF/perovskite/TPBi/LiF/Al were fabricated. The device structure and energy levels are diagrammatically shown in Fig. 3(a) and (b), respectively. A cross-section scanning electron microscope (SEM) image of the PeLED modified with 2 nm LiF is shown in Fig. 3(c). The EL spectra of PeLEDs modified with 2 nm LiF under different voltage biases are given in Fig. 3(d). All PeLEDs modified with LiF layers exhibit a pure green EL peak at 532 nm with narrow FWHM of 22 nm, suggesting a high color purity for display applications. Furthermore, the EL peak remains unchanged and symmetrical as the voltage increases from 5 V to 9 V, indicating a stable crystal phase under working condition. The EL peak shift usually happens in the mix-halide perovskite system due to the halide migration. The stable EL peak position when increasing the applied bias demonstrates that little Li^+ or F^- incorporated into the perovskite crystal lattice, as the ionic radii of Li^+ and F^- is too small to fit the tolerance factor and form stable perovskite structure. Fig. 3(e–g) show the voltage-dependent luminance, current density, and current efficiency (CE) of PeLEDs modified with different thicknesses of LiF layers. In Fig. 3(e), the control device exhibits the lowest luminance (<100 cd/m^2) and the highest turn-on voltage (the voltage when luminance>1 cd/m^2) of 4.9 V. The poor EL performance of the control device is due to leakage current. As shown in Fig. 3(f), the current density of the control device remains at a high level even though the applied voltage is below the turn-on voltage, indicating a high level of leakage current that originates from the pinhole defects of the perovskite film. However, very low current is observed below the turn-on voltage after modification with the LiF layer, demonstrating that the leakage current is effectively suppressed by the morphology improvement. In addition, the device exhibits a large enhancement in the maximum luminance (3271 cd/m^2), CE (1 cd/A), and a lowered turn-on voltage (2.8 V) when a 1 nm LiF layer is inserted. The optimal EL performance is obtained by increasing the LiF thickness to 2 nm, at which the highest luminance of 10415 cd/m^2, maximum CE of 12.1 cd/A, and EQE of 3.5% are exhibited. These performances are 100-fold over than the references.

Table 1
PL lifetime and diffraction of perovskite film on substrates without and with different thicknesses of LiF layer, obtained from the fitting curves using a bi-exponential decay model.

Sample	τ_1 (ns)	f_1 (%)	τ_2 (ns)	f_2 (%)	τ_{avg} (ns)
w/o LiF	4.1	78.9	45.1	21.1	12.8
1 nm LiF	5.7	73.1	49.5	26.9	17.5
2 nm LiF	6.8	65.4	61.2	34.6	25.6
3 nm LiF	6.3	70.8	82.4	29.2	28.5
4 nm LiF	9.0	60.7	136.5	39.3	59.1

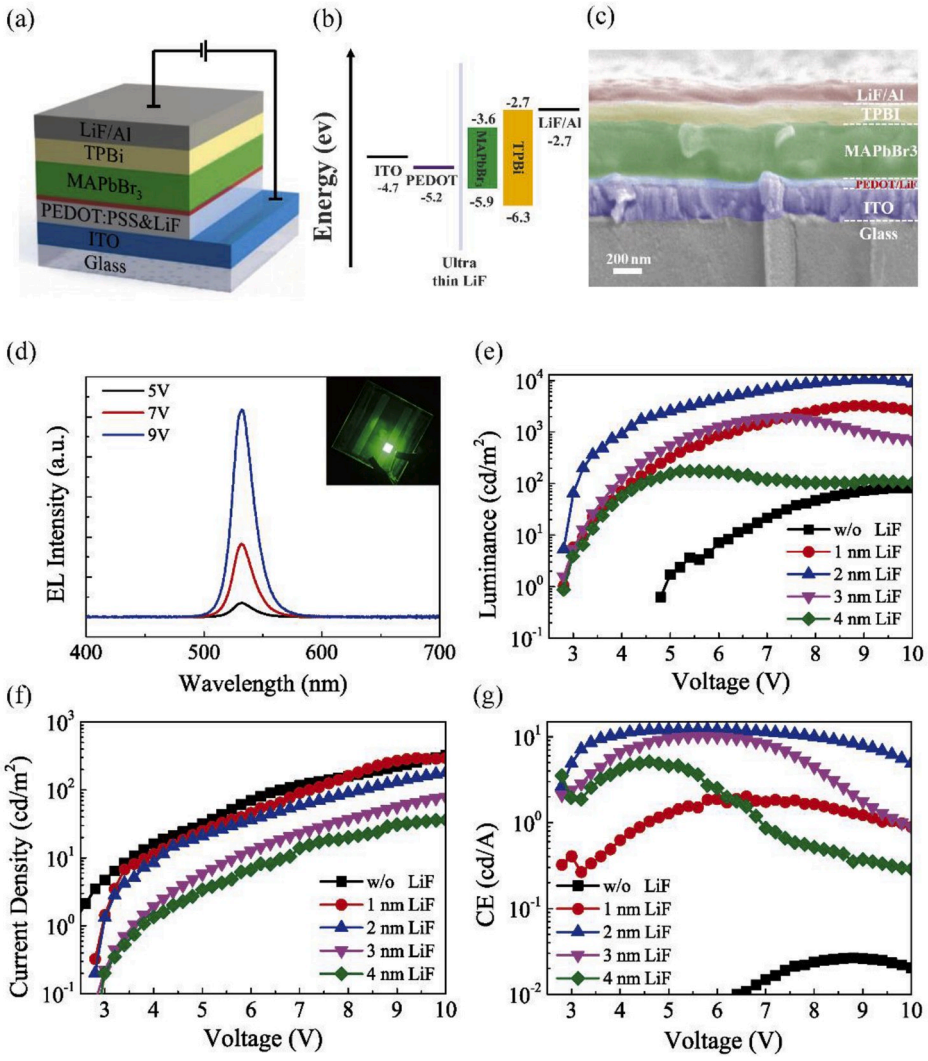

Fig. 3. (a) Structure diagram and (b) energy band alignment of PeLED with LiF modified layer. (c) Cross-section SEM image of PeLED modified with 2 nm LiF layer. (d) EL spectral of the PeLEDs at various applied voltages. The emission image of the device with 2 nm thick LiF is shown in inset. (e) L-V, (f) J-V and (g) CE-V spectra of PeLEDs with LiF thicknesses varying from 0 nm to 4 nm.

The reason for the relatively poor performance of device with 1 nm LiF can be refer to the severe exciton quenching and the large existence of electron trap-states. According to the preceding discussion on the interface passivation effect introduced by the LiF layer, the improved EL performance originates mainly from the reduction of trap density and exciton quenching at the PEDOT:PSS/perovskite interface, and the resulting increase in radiative recombination. The operational stability for device with 2 nm LiF layer was test, as shown in Fig. S6. The device was tested at an initial luminance of 100 cd/m^2, and the time for the luminance declined by half can be regarded as the reference of operational stability. It took 16.6 min for the luminance declined by half for device with 2 nm LiF layer, while the controlled device burned out in several seconds with a much lower initial luminance.

However, the luminance degrades as the LiF thickness increases beyond 3 nm as shown in Fig. 3(e). The luminance is 1938 cd/m^2 and 174 cd/m^2 for PeLEDs modified with 3 nm and 4 nm LiF layers, respectively. The EL parameters of PeLEDs without and with varied thickness of LiF are listed in Table 2. Some possible explanations for the luminance reduction are as follows. Firstly, the increased surface roughness of PEDOT:PSS/LiF film, as shown in Fig. 1(f), leads to inferior ohmic contact between the PEDOT:PSS/LiF substrate and the perovskite film. Secondly, the tunneling effect through the ultrathin LiF layer is eliminated as the thickness increases. The insulator property of the LiF layers impedes electron/hole injection, thereby decreasing the current density when the LiF thickness increases, as shown in Fig. 3(f). It is important to note that the PeLED with 1 nm LiF layer exhibits higher luminance than that with 4 nm LiF layer, as shown in Fig. 3(e). However, the 4 nm LiF layer still contributes to a higher CE when the voltage is below 5 V. The enhanced CE is mainly due to the reduced trap density at the PEDOT:PSS/perovskite interface. When the voltage is over 5 V, the luminance and CE of PeLEDs modified with 3 nm and 4 nm LiF layers drop significantly. The large reduction probably originates from the increased joule heating by the increased series resistance of the device. To confirm this hypothesis, impedance measurement of PeLEDs with

Table 2
EL parameters for PeLEDs without and with varied thickness of LiF inserting layer.

Sample	L_{max} [cd/m^2]	CE_{max} [cd/A]	EQE_{max} [%]	Turn-on voltage [V]
w/o LiF	82	0.026	0.007	4.9
1 nm LiF	3271	2.0	0.58	2.8
2 nm LiF	10415	12.1	3.5	2.8
3 nm LiF	1938	10.1	2.9	2.8
4 nm LiF	174	5.1	1.5	2.8

different thicknesses of LiF layers was carried out (Fig. S4). All devices were tested with applied bias at turn-on voltage (4.9 V and 2.8 V for PeLED without and with LiF layers, respectively). The radius of the Nyquist plot enlarges as the LiF thickness increases, indicating an increased series resistance of the PeLEDs due to the increased insulator property of thicker LiF layers.

Similar to the luminance, the CE decreases when the LiF thickness is larger than 3 nm as shown in Fig. 4(d). Generally, an unbalanced charge injection can bring about charge carrier accumulation at the interface, resulting in the shifting away of the recombination zone away from the perovskite layer and hence a reduction of the CE. The influence of LiF modified layers on the charge injection equilibrium of current injection is therefore further investigated. Electron-only and hole-only devices with different thicknesses of LiF layers were fabricated as per the earlier discussion on the electron/hole trap states. It should be mentioned that when the applied voltage surpasses 5 V, the perovskite films of the electron-only devices tend to burn up due to the high current density which originates from the high electron conductivity of the TPBi and ZnO layers. As a result, the J-V characteristics of the single carrier devices is measured with applied voltage under 5 V. The J-V characteristics of electron-only devices (ITO/ZnO/LiF/perovskite/TPBi/LiF/Al) and hole-only devices (ITO/PEDOT/LiF/perovskite/Ag) with different LiF thicknesses are shown in Fig. 4(a) and Fig. 4(b), respectively. Both the electron and hole current density generally decrease as the thicknesses of the LiF layers increase. The current density decrease can be attributed to the increased insulating ability of thicker LiF layers. The current densities of electron-only devices are compared with those of hole-only devices with the same LiF thickness, as shown in Fig. 4(c) and Fig. S6. For the control group without LiF layer (Fig. S6(a)), the electron current density is ~2 times higher than the hole current density. This is because the disparity between the work function of PEDOT:PSS (~4.9 eV) and the highest unoccupied molecular orbital (HOMO, ~5.7 eV) is so large that the transportation of hole current is hindered, even though $MAPbBr_3$ has been confirmed to be a P type semiconductor. After inserting the LiF modified layers, the disparity between the electron and hole current density is decreased. In particular, the current density of electron-only and hole-only devices become nearly identical with 2 nm LiF layers as shown in Fig. 4(c), indicating balanced charge injection. However, the hole current density surpasses the electron current density when the LiF thickness becomes larger than 3 nm (Fig. S6(c)), and becomes dominant when the LiF thickness is 4 nm (Fig. S6(d)). These trends are due to the significant enhancement of the electron blockage with increasing LiF thickness while the obstruction to hole injection is limited — the change in electron current is one order of magnitude larger than the change in hole current. Consequently, balanced current injection is reached using 2 nm LiF layers, which is consistent with the PeLED with the best EL performance.

Previous research on organic LEDs and polymer LEDs have proven that the inserted thin LiF layer between the ITO and emitting layer can effectively improve the hole current density. This improvement is attributed to the tunneling effect [38,39]. The tunneling effect is significant for hole current injection only for a large energy barrier. For a small energy barrier, the insulator property of LiF plays the leading role in hindering the hole injection. In our experiments, the hole current density decreases with increasing LiF thickness, indicating that the enhancement of EL performance by inserting a thin LiF layer does not originate from the tunneling effect. This is mainly because the energy offset between the WF of PEDOT:PSS and the HOMO of $MAPbBr_3$ is not large enough. To further investigate this issue, ITO/LiF substrates with large energy barriers between the Fermi level of ITO (~4.8 eV) and the HOMO (~5.7 eV) of the perovskite layers were used to fabricate PeLEDs. The EL performances of devices deposited on ITO/LiF substrates are

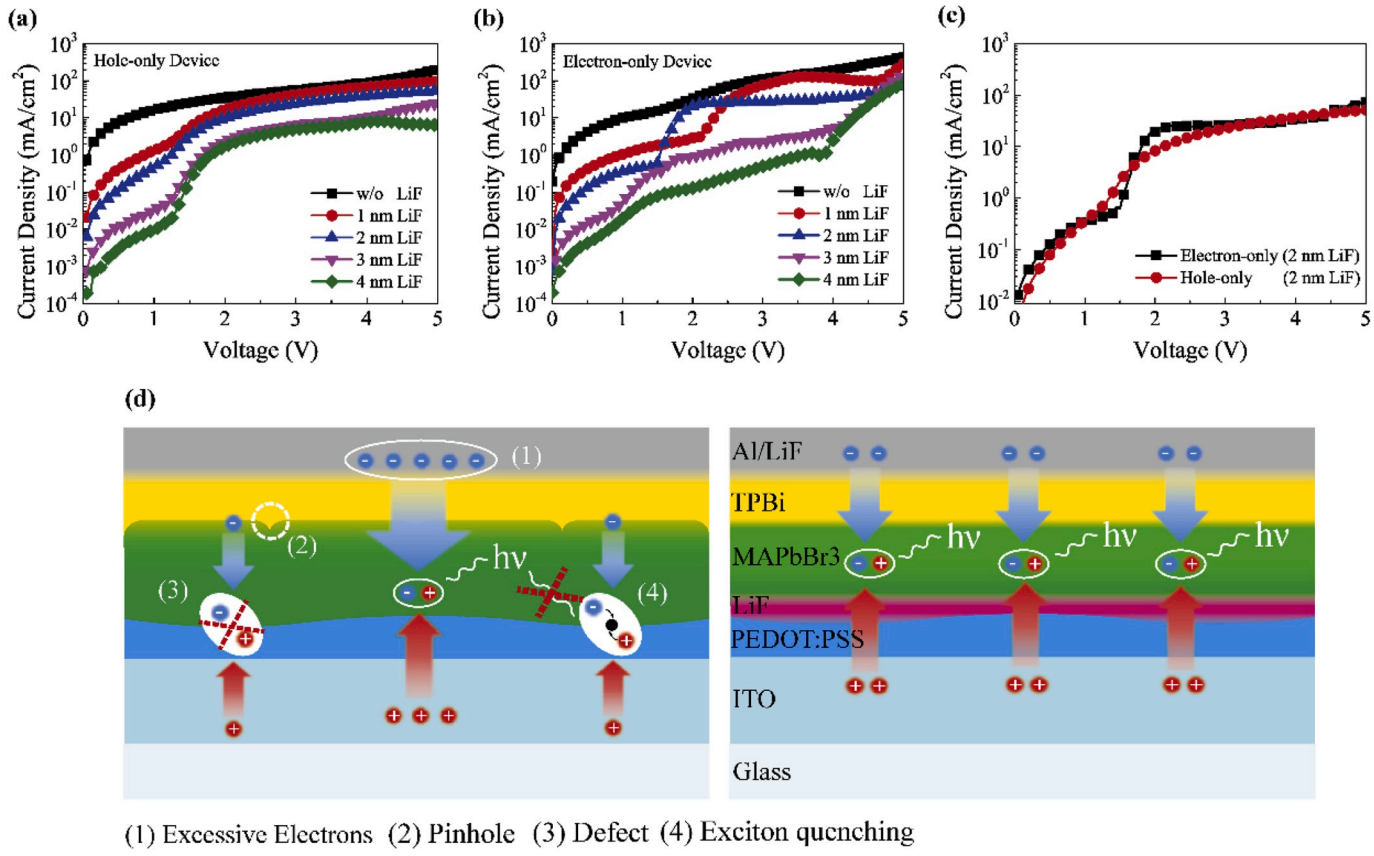

Fig. 4. J-V curves of (a) electron-only and (b) hole-only device with LiF thickness varying from 0 nm to 4 nm. (c) Selective comparison of J-V curves of electron-only and hole-only devices with 2 nm thick LiF. (d) The working mechanism of device without and with LiF layer.

shown in Fig. S4. The maximum luminance of the best device is 6713.9 cd/m^2 with a turn-on voltage of 3.8 V, while the control device without LiF shows a poor maximum luminance of 879.5 cd/m^2 with high turn-on voltage of 4.6 V. Although the LiF is also present at the interface of ITO/perovskite film, the maximum luminance and turn-on voltage achieved are still far inferior to the PeLEDs on ITO/PEDOT:PSS/LiF substrates. Moreover, the current efficiency of 3.1 cd/A for PeLEDs deposited on ITO/LiF substrates is also lower than our optimal PeLEDs. The current density of PeLEDs deposited on ITO/LiF and ITO/PEDOT:PSS/LiF substrates are given in Fig. S6. The current density of PeLEDs deposited on ITO/PEDOT:PSS/LiF substrates is much higher than the PeLEDs without PEDOT:PSS regardless of the LiF layer thickness. These results can be attributed to the insufficient hole injection without PEDOT:PSS despite the tunneling effect at the large energy barrier of the LiF layer. Consequently, the EL enhancement resulting from the tunneling effect of the LiF layer through a large energy barrier, such as that in the ITO/perovskite in the previous study [40], is not comparable with the EL enhancement achieved by introducing a PEDOT:PSS/LiF hybrid layer. The working mechanism of the devices modified without and with the LiF layer is shown in Fig. 4(d). The improved performance of our optimal PeLEDs is mainly due to the modified morphology, interface passivation effect, and balanced injection discussed above. It is important to note that our work mainly focuses on the modification of the interface between PEDOT:PSS and the perovskite layer, and the device efficiency can be further improved by passivation at the grain boundaries of the perovskite layer through various means such as doping, alloying, and polymer blending [41].

4. Conclusions

In summary, a facile and effective interface modification method that involves inserting an ultrathin LiF layer between the PEDOT:PSS and perovskite film is presented. By inserting a LiF modified layer, better perovskite film surface morphology is achieved owing to the improved surface roughness and wettability of PEDOT:PSS. Steady-state and time-resolved PL measurements confirm the effective suppression of exciton quenching by the conductive PEDOT chains with increasing LiF thickness. The reduced electron and hole trap densities at the interface of the perovskite film are also confirmed by calculations from the dark J-V measurement. The above results indicate a dual-passivation effect of the LiF layers on both PEDOT:PSS and perovskite interfaces. We further investigate the charge injection properties of electron-only and hole-only devices modified with LiF layers. The results suggest that both electron and hole current densities decrease with increasing LiF layer thickness. Moreover, equilibrium between the electron and hole current injection can be achieved by tuning the thickness of LiF due to the preferential hinderance of electron current compared to hole current. The optimal PeLED with a 2 nm thick LiF layer exhibits a maximum luminance, current efficiency and EQE of 10415 cd/m^2, 12.1 cd/A and 3.5%, respectively, with a decreased turn-on voltage of 2.8 V compared to the 4.9 V of the pristine device.

Declaration of competing interest

The authors declare that they have no known competing financial interests or personal relationships that could have appeared to influence the work reported in this paper.

Acknowledgements

This work is supported by the Natural Science Foundation of Guangdong Province (2018B030306008); National Natural Science Foundation of China (51735004) and Science & Technology Program of Guangdong Province (2017B010115001, 2016B010130001).

Appendix A. Supplementary data

Supplementary data to this article can be found online at https://doi.org/10.1016/j.orgel.2020.105675.

References

[1] H. Cho, S.H. Jeong, M.H. Park, Y.H. Kim, C. Wolf, C.L. Lee, J.H. Heo, A. Sadhanala, N. Myoung, S. Yoo, S.H. Im, R.H. Friend, T.W. Lee, Overcoming the electroluminescence efficiency limitations of perovskite light-emitting diodes, Science 350 (2015) 1222–1225, https://doi.org/10.1126/science.aad1818.
[2] Z. Li, Z. Chen, Y. Yang, Q. Xue, H.L. Yip, Y. Cao, Modulation of recombination zone position for quasi-two-dimensional blue perovskite light-emitting diodes with efficiency exceeding 5%, Nat. Commun. 10 (2019) 1027, https://doi.org/10.1038/s41467-019-09011-5.
[3] Z. Li, C. Song, J. Li, G. Liang, L. Rao, S. Yu, X. Ding, Y. Tang, B. Yu, J. Ou, U. Lemmer, G. Gomard, Highly efficient and water-stable lead halide perovskite quantum dots using superhydrophobic aerogel inorganic matrix for white light-emitting diodes, Adv. Mater. Technol. (2020) 1900941, https://doi.org/10.1002/admt.201900941.
[4] H. Zhou, Q. Chen, G. Li, S. Luo, T.-b. Song, H.-S. Duan, Z. Hong, J. You, Y. Liu, Y. Yang, Interface engineering of highly efficient perovskite solar cells, Science 345 (2014) 542–546, https://doi.org/10.1126/science.1254050.
[5] D. Shin, D. Kang, J.B. Lee, J.H. Ahn, I.W. Cho, M.Y. Ryu, S.W. Cho, N.E. Jung, H. Lee, Y. Yi, Electronic structure of nonionic surfactant-modified PEDOT:PSS and its application in perovskite solar cells with reduced interface recombination, ACS Appl. Mater. Interfaces 11 (2019) 17028–17034, https://doi.org/10.1021/acsami.9b01545.
[6] Q. Jiang, Y. Zhao, X. Zhang, X. Yang, Y. Chen, Z. Chu, Q. Ye, X. Li, Z. Yin, J. You, Surface passivation of perovskite film for efficient solar cells, Nat. Photon. 13 (2019) 460, https://doi.org/10.1038/s41566-019-0462-y.
[7] L. Dou, Y. Yang, J. You, Z. Hong, W.-H. Chang, G. Li, Y. Yang, Solution-processed hybrid perovskite photodetectors with high detectivity, Nat. Commun. 5 (2014) 5404, https://doi.org/10.1038/s41467-019-09822-6.
[8] C. Li, C. Han, Y. Zhang, Z. Zang, M. Wang, X. Tang, J. Du, Enhanced photoresponse of self-powered perovskite photodetector based on ZnO nanoparticles decorated CsPbBr3 films, Sol. Energy Mater. Sol. Cells 172 (2017) 341–346, https://doi.org/10.1016/j.solmat.2017.08.014.
[9] S.-F. Leung, K.-T. Ho, P.-K. Kung, V.K.S. Hsiao, H.N. Alshareef, Z.L. Wang, J.-H. He, A self-powered and flexible organometallic halide perovskite photodetector with very high detectivity, Adv. Mater. 30 (2018) 1704611, https://doi.org/10.1002/adma.201704611.
[10] Y. Cao, N. Wang, H. Tian, J. Guo, Y. Wei, H. Chen, Y. Miao, W. Zou, K. Pan, Y. He, H. Cao, Y. Ke, M. Xu, Y. Wang, M. Yang, K. Du, Z. Fu, D. Kong, D. Dai, Y. Jin, G. Li, H. Li, Q. Peng, J. Wang, W. Huang, Perovskite light-emitting diodes based on spontaneously formed submicrometre-scale structures, Nature 562 (2018) 249–253, https://doi.org/10.1038/s41586-018-0576-2.
[11] M.H. Park, J. Park, J. Lee, H.S. So, H. Kim, S.H. Jeong, T.H. Han, C. Wolf, H. Lee, S. Yoo, T.W. Lee, Efficient perovskite light-emitting diodes using polycrystalline core–shell-mimicked nanograins, Adv. Funct. Mater. 29 (2019) 1902017, https://doi.org/10.1002/adfm.201902017.
[12] Q. Zhang, M.M. Tavakoli, L. Gu, D. Zhang, L. Tang, Y. Gao, J. Guo, Y. Lin, S. F. Leung, S. Poddar, Y. Fu, Z. Fan, Efficient metal halide perovskite light-emitting diodes with significantly improved light extraction on nanophotonic substrates, Nat. Commun. 10 (2019) 727, https://doi.org/10.1038/s41467-019-08561-y.
[13] K. Lin, J. Xing, L.N. Quan, F.P.G. de Arquer, X. Gong, J. Lu, L. Xie, W. Zhao, D. Zhang, C. Yan, W. Li, X. Liu, Y. Lu, J. Kirman, E.H. Sargent, Q. Xiong, Z. Wei, Perovskite light-emitting diodes with external quantum efficiency exceeding 20 per cent, Nature 562 (2018) 245–248, https://doi.org/10.1038/s41586-018-0575-3.
[14] W. Xu, Q. Hu, S. Bai, C. Bao, Y. Miao, Z. Yuan, T. Borzda, A.J. Barker, E. Tyukalova, Z. Hu, M. Kawecki, H. Wang, Z. Yan, X. Liu, X. Shi, K. Uvdal, M. Fahlman, W. Zhang, M. Duchamp, J.-M. Liu, A. Petrozza, J. Wang, L.-M. Liu, W. Huang, F. Gao, Rational molecular passivation for high-performance perovskite light-emitting diodes, Nat. Photon. 13 (2019) 418, https://doi.org/10.1038/s41566-019-0390-x.
[15] Z.T. Li, K. Cao, J.S. Li, Y. Tang, L. Xu, X.R. Ding, B.H. Yu, Investigation of light-extraction mechanisms of multiscale patterned arrays with rough morphology for GaN-based thin-film LEDs, IEEE Access 7 (2019) 73890–73898, https://doi.org/10.1109/ACCESS.2019.2921058.
[16] X. Sun, C. Han, K. Wang, H. Yu, J. Li, K. Lu, J. Qin, H. Yang, L. Deng, F. Zhao, Q. Yang, B. Hu, Effect of bathocuproine organic additive on optoelectronic properties of highly efficient methylammonium lead bromide perovskite light-emitting diodes, ACS Appl. Energy Mater. 1 (2018) 6992–6998, https://doi.org/10.1021/acsaem.8b01410.
[17] H. Zhang, F. Ye, W. Li, R.S. Gurney, D. Liu, C. Xiong, T. Wang, Improved performance of perovskite light-emitting diodes by dual passivation with an ionic additive, ACS Appl. Energy Mater. 2 (2019) 3336–3342, https://doi.org/10.1021/acsaem.9b00186.
[18] Y. Zou, M. Ban, Y. Yang, S. Bai, C. Wu, Y. Han, T. Wu, Y. Tan, Q. Huang, X. Gao, T. Song, Q. Zhang, B. Sun, Boosting perovskite light-emitting diode performance via tailoring interfacial contact, acs applied materials & interfaces, ACS Appl. Mater. Interfaces 10 (2018) 24320–24326, https://doi.org/10.1021/acsami.8b07438.

[19] L. Tang, J. Qiu, Q. Wei, H. Gu, B. Du, H. Du, W. Hui, Y. Xia, Y. Chen, W. Huang, Enhanced performance of perovskite light-emitting diodes via diamine interface modification, ACS Appl. Mater. Interfaces 11 (2019) 29132–29138, https://doi.org/10.1021/acsami.9b11866.
[20] B.R. Lee, J.C. Yu, J.H. Park, S. Lee, C.K. Mai, B. Zhao, M.S. Wong, E.D. Jung, Y. S. Nam, S.Y. Park, D. Di Nuzzo, J.Y. Kim, S.D. Stranks, G.C. Bazan, H. Choi, M. H. Song, R.H. Friend, Conjugated polyelectrolytes as efficient hole transport layers in perovskite light-emitting diodes, ACS Nano 12 (2018) 5826–5833, https://doi.org/10.1021/acsnano.8b01715.
[21] Y. Liu, T. Wu, Y. Liu, T. Song, B. Sun, Suppression of non-radiative recombination toward high efficiency perovskite light-emitting diodes, Apl. Mater. 7 (2019), 021102, https://doi.org/10.1063/1.5064370.
[22] Q. Lin, A. Armin, R.C.R. Nagiri, P.L. Burn, P. Meredith, Electro-optics of perovskite solar cells, Nat. Photon. 9 (2015) 106–112, https://doi.org/10.1038/NPHOTON.2014.284.
[23] D.-Y. Lee, S.-I. Na, S.-S. Kim, Graphene oxide/PEDOT:PSS composite hole transport layer for efficient and stable planar heterojunction perovskite solar cells, Nanoscale 8 (2016) 1513–1522, https://doi.org/10.1039/c5nr05271h.
[24] P. Chen, Z. Xiong, X. Wu, M. Shao, Y. Meng, Z.-h. Xiong, C. Gao, Nearly 100% efficiency enhancement of CH3NH3PbBr3 perovskite light-emitting diodes by utilizing plasmonic Au nanoparticles, J. Phys. Chem. Lett. 8 (2017) 3961–3969, https://doi.org/10.1021/acs.jpclett.7b01562.
[25] Y. Meng, M. Ahmadi, X. Wu, T. Xu, L. Xu, Z. Xiong, P. Chen, High performance and stable all-inorganic perovskite light emitting diodes by reducing luminescence quenching at PEDOT:PSS/Perovskites interface, Org. Electron. 64 (2019) 47–53, https://doi.org/10.1016/j.orgel.2018.10.014.
[26] J. Wang, C. Song, Z. He, C. Mai, G. Xie, L. Mu, Y. Cun, J. Li, J. Wang, J. Peng, Y. Cao, All-solution-Processed pure formamidinium-based perovskite light-emitting diodes, Adv. Mater. 30 (2018), e1804137, https://doi.org/10.1002/adma.201804137.
[27] X.F. Peng, X.Y. Wu, X.X. Ji, J. Ren, Q. Wang, G.Q. Li, X.H. Yang, Modified conducting polymer hole injection layer for high-efficiency perovskite light-emitting devices: enhanced hole injection and reduced luminescence quenching, J. Phys. Chem. Lett. 8 (2017) 4691–4697, https://doi.org/10.1021/acs.jpclett.7b01992.
[28] J.C. Yu, D.W. Kim, D.B. Kim, E.D. Jung, K.S. Lee, S. Lee, D.D. Nuzzo, J.S. Kim, M. H. Song, Effect of the solvent used for fabrication of perovskite films by solvent dropping on performance of perovskite light-emitting diodes, Nanoscale 9 (2017) 2088–2094, https://doi.org/10.1039/c6nr08158d.
[29] Q.-W. Liu, S. Yuan, S.-Q. Sun, W. Luo, Y.-J. Zhang, L.-S. Liao, M.-K. Fung, Interfacial engineering for highly efficient quasi-two dimensional organic–inorganic hybrid perovskite light-emitting diodes, J. Mater. Chem. C 7 (2019) 4344–4349, https://doi.org/10.1039/c8tc06490c.
[30] S. Ma, W. Qiao, T. Cheng, B. Zhang, J. Yao, A. Alsaedi, T. Hayat, Y. Ding, Z. Tan, S. Dai, Optical-electrical-chemical engineering of PEDOT:PSS by incorporation of hydrophobic nafion for efficient and stable perovskite solar cells, ACS Appl. Mater. Interfaces 10 (2018) 3902–3911, https://doi.org/10.1021/acsami.7b19053.
[31] X. Liu, X. Guo, Y. Lv, Y. Hu, Y. Fan, J. Lin, X. Liu, X. Liu, High brightness and enhanced stability of CsPbBr3-based perovskite light-emitting diodes by morphology and interface engineering, Adv. Opt. Mater. 6 (2018) 1801245, https://doi.org/10.1002/adom.201801245.
[32] S.-H. Jeong, H. Kim, M.-H. Park, Y. Lee, N. Li, H.-K. Seo, T.-H. Han, S. Ahn, J.-M. Heo, K.S. Kim, T.-W. Lee, Ideal conducting polymer anode for perovskite light-emitting diodes by molecular interaction decoupling, Nano Energy 60 (2019) 324–331, https://doi.org/10.1016/j.nanoen.2019.03.030.
[33] X. Zhang, H. Liu, W. Wang, J. Zhang, B. Xu, K.L. Karen, Y. Zheng, S. Liu, S. Chen, K. Wang, X.W. Sun, Hybrid perovskite light-emitting diodes based on perovskite nanocrystals with organic-inorganic mixed cations, Adv. Mater. 29 (2017) 1606405, https://doi.org/10.1002/adma.201702815.
[34] V. Prakasam, F. Di Giacomo, R. Abbel, D. Tordera, M. Sessolo, G. Gelinck, H. J. Bolink, Efficient perovskite light-emitting diodes: effect of composition, morphology, and transport layers, ACS Appl. Mater. Interfaces 10 (2018) 41586–41591, https://doi.org/10.1021/acsami.8b15718.
[35] J. Song, J. Li, L. Xu, J. Li, F. Zhang, B. Han, Q. Shan, H. Zeng, Room-temperature triple-ligand surface engineering synergistically boosts ink stability, recombination dynamics, and charge injection toward EQE-11.6% perovskite QLEDs, Adv. Mater. 30 (2018) 1800764, https://doi.org/10.1002/adma.201800764.
[36] S. Yuan, Z.-K. Wang, M.-P. Zhuo, Q.-S. Tian, Y. Jin, L.-S. Liao, Self-assembled high quality CsPbBr3 quantum dot films toward highly efficient light-emitting diodes, ACS Nano 12 (2018) 9541–9548, https://doi.org/10.1021/acsnano.8b05185.
[37] Y. Liu, Y. Zhang, K. Zhao, Z. Yang, J. Feng, X. Zhang, K. Wang, L. Meng, H. Ye, M. Liu, S. Liu, A 1300 mm(2) ultrahigh-performance digital imaging assembly using high-quality perovskite single crystals, Adv. Mater. 30 (2018) 1707314, https://doi.org/10.1002/adma.201707314.
[38] F.R. Zhu, B.L. Low, K.R. Zhang, S.J. Chua, Dual role of LiF as a hole-injection buffer in organic light-emitting diodes, Appl. Phys. Lett. 79 (2001) 1205–1207, https://doi.org/10.1063/1.1695444.
[39] J.M. Zhao, S.T. Zhang, X.J. Wang, Y.Q. Zhan, X.Z. Wang, G.Y. Zhong, Z.J. Wang, X. M. Ding, W. Huang, X.Y. Hou, Lithium-fluoride-modified indium tin oxide anode for enhanced carrier injection in phenyl-substituted polymer electroluminescent devices, Appl. Phys. Lett. 84 (2004) 2913–2915, https://doi.org/10.1063/1.1396819.
[40] Y. Shi, W. Wu, H. Dong, G. Li, K. Xi, G. Divitini, C. Ran, F. Yuan, M. Zhang, B. Jiao, X. Hou, Z. Wu, A strategy for architecture design of crystalline perovskite light-emitting diodes with high performance, Adv. Mater. 30 (2018) 1800251, https://doi.org/10.1002/adma.201800251.
[41] M. Lu, Y. Zhang, S. Wang, J. Guo, W.W. Yu, A.L. Rogach, Metal halide perovskite light-emitting devices: promising Technology for next-generation displays, Adv. Funct. Mater. 29 (2019) 1902008, https://doi.org/10.1002/adfm.201902008.